



Climate response to the spatial and temporal evolutions of anthropogenic aerosol forcing

Hai Wang¹ · Yu-Jun Wen¹

Received: 19 May 2021 / Accepted: 12 November 2021 / Published online: 24 November 2021
© The Author(s), under exclusive licence to Springer-Verlag GmbH Germany, part of Springer Nature 2021

Abstract

Large-scale climate response to the spatial and temporal changes of anthropogenic aerosols are investigated in comparison with greenhouse gas (GHG) forcing using Coupled Model Intercomparison Project Phase 6 (CMIP6) simulations during 1930–2010. Globally, increasing anthropogenic aerosols in the Northern Hemisphere (NH) since the industrial revolution generates a North–South interhemispherically asymmetric climate response pattern. But this feature only dominates the historical climate change early in the twentieth century. In the second half of the twentieth century, anthropogenic aerosol emissions increase monotonically in Asia, but increase first and then decrease rapidly over Europe and North America. The shift of aerosol emissions from the western mid-latitude NH to the eastern low-latitude NH induces distinct climate response patterns compared with its global increase effect, anchoring an equatorial symmetric tropical sea surface temperature (SST) cooling and precipitation decrease, which resembles that in the GHG-induced response patterns with sign reversed. After the mid-1970s, with declining aerosol emissions over Europe and North America and increasing emissions in Asia, anthropogenic aerosol forcing generates a northward recovery of the tropical rainfall with little response in the tropical SST anomalies due to the cancellation effect of the distinct aerosol emissions conditions between the western and the eastern NH. While GHG forcing dominates observed climate change in the twentieth century, the distinct climate response patterns to the spatial and temporal evolutions of anthropogenic aerosol forcing highlight its important role in shaping the regional climate changes.

Keywords Aerosol forcing · Spatial variation · Temporal evolution · Climate response · Atmospheric circulation

1 Introduction

Since the industrial revolution, dramatic increase in greenhouse gases (GHG) and anthropogenic aerosols have been the dominant drivers of forced climate change on both global and regional scales, with each having opposite effects on the Earth's radiative energy balance (Myhre et al. 2013; Bellouin et al. 2020). In the 5th Assessment Report from the Intergovernmental Panel on Climate Change (Myhre et al. 2013), the radiative forcing change due to historical increase in the concentration of GHG was estimated to be 2.83 Wm^{-2} (from 2.54 to 3.12 Wm^{-2}); the total aerosol effect (excluding black carbon on snow and ice) was estimated as an effective radiative forcing of -0.9 Wm^{-2} (from -1.9 to -0.1

Wm^{-2}), masking about one-third of the GHG-induced warming. GHG modulate the atmospheric energy balance through the absorption of longwave radiation and warm the atmosphere. Anthropogenic aerosols, including both absorbing (i.e. black carbon) and scattering (i.e. sulfate) species, influence shortwave radiation and further change the energy budget of the climate system (known as the “direct effect” Menon et al. 2002). Aerosols can also serve as cloud condensation nuclei which affect the cloud albedo, as well as the cloud lifetime and precipitation efficiency (known as the “first indirect effect” and “second indirect effect” (Twomey 1977; Albrecht 1989; Levy et al. 2013; Bellouin et al. 2020). With distinct radiative impacts, GHG and anthropogenic aerosols have opposite signed effects on the global mean surface temperature change (Forster et al. 2007). Due to polar amplification and the larger response over land than ocean, the surface air temperature response to GHG and aerosol forcing show some resemblance to each other (Boer and Yu 2003). Furthermore, Xie et al. (2013) also noted that the GHG and aerosol forcing can induce similar spatial patterns

✉ Hai Wang
wanghai@ouc.edu.cn

¹ Physical Oceanography Laboratory, and College of Oceanic and Atmospheric Sciences, Ocean University of China, Qingdao 266100, China

of tropical sea surface temperature (SST) and precipitation responses with sign reversed due to the common global mode of radiative-induced climate change.

More importantly, GHG and anthropogenic aerosols differ not only in their global mean radiative forcing impacts, but also in their spatial and temporal evolutions. Unlike the long-lived GHG, anthropogenic aerosols are geographically inhomogeneous due to their short atmospheric residence time. Since the industrial revolution, emissions of anthropogenic aerosols changed significantly over Asia, Europe and North America (EU&NA) with varying spatial patterns and time evolutions. On the other hand, the GHG change is globally well-mixed, and monotonically increased. These distinct forcing characters complicate the study of regional and global climate response to anthropogenic aerosol and GHG changes.

Using coupled climate models, atmospheric general circulation models (AGCM), as well as theoretical considerations, the physical mechanisms of long-term large-scale climate response to anthropogenic aerosol forcing have been investigated. On regional scale, anthropogenic aerosols can cause atmospheric circulation changes wherever the aerosol concentrations are high. During the twentieth century, anthropogenic aerosols increase most in Asia. Thus, the impacts of anthropogenic aerosols on Asian summer monsoon have drawn much attention in recent years (Li et al. 2016). Anthropogenic aerosols can affect the local precipitation and atmospheric circulation directly by modifying the radiation and cloud physics (Menon et al. 2002; Ramanathan et al. 2005; Lau et al. 2006; Rosenfeld et al. 2008; Bollasina et al. 2013; Li et al. 2018), leading to the adjustments of local meridional overturning circulations and the corresponding monsoon rainfall response. The aerosol forcing can weaken the South Asian summer monsoon via a SST-mediated response by weakening the global tropical meridional overturning circulation, which response to the aerosol-induced energy imbalance between the Northern Hemisphere (NH) and the Southern Hemisphere (SH) (Bollasina et al. 2011; Ganguly et al. 2012; Wang et al. 2019) with some contribution from the spatial pattern of SST response (Wang et al. 2019). Recent studies (Wang et al. 2019; Li et al. 2020) indicate that the direct atmospheric response plays a dominant role in weakening the East Asian summer monsoon in part by reducing the land-sea thermal contrast (Song et al. 2014).

Another striking regional climate response to anthropogenic aerosol forcing is Sahel rainfall change in the second half of the twentieth century. Emissions of anthropogenic aerosols from EU&NA increase steadily from the industrial revolution until the mid-1970s, and then rapidly decrease due to emission regulations to the early twentieth century levels by recent times. Such time-evolving change of anthropogenic aerosols leads to a reversal in pattern of

Sahel rainfall response through either direct atmospheric radiative forcing effect (Dong et al. 2014; Hirasawa et al. 2020) or by modulating the SST anomaly pattern and the corresponding atmospheric circulation change (Booth et al. 2012; Haywood et al. 2013; Dong and Sutton 2015; Giannini and Kaplan 2019; Hirasawa et al. 2020). A recent study also noted EU&NA aerosol forcing related multidecadal variations across all ocean basins since 1920 (Qin et al. 2020). Furthermore, the aerosol forcing from EU emissions may also influence the Asian summer monsoon response by modulating mid-latitude tropospheric temperatures and westerly jet anomalies (Undorf et al. 2018).

Globally, constrained by cross-equatorial energy transport balance theory (Kang et al. 2008; Chiang and Friedman 2012), the aerosol-induced NH SST and tropospheric cooling can cause an interhemispherically asymmetric climate response, including an anomalous cross-equatorial meridional overturning circulation and corresponding southward shift of the inter tropical convergence zone (ITCZ) (Rotstayn and Lohmann 2002; Hwang et al. 2013; Allen et al. 2015; Wang et al. 2016a, b; Soden and Chung 2017). In contrast, on the zonal mean view, the GHG-induced tropical atmospheric circulation and precipitation responses are more symmetric about the equator, and which are mediated by the “wet-get-wetter” and “warmer-get-wetter” jointly (Held and Soden 2006; Xie et al. 2010; Huang et al. 2013). In addition to the tropical response, anthropogenic aerosol forcing also induces significant mid-latitude westerly jet responses in both hemispheres. For the NH, the westerly jet is shifted southward due to both geostrophic balancing of the northern branch of the aerosol-induced anomalous cross-equatorial meridional overturning circulation as well as thermal wind balancing of the NH mid-latitude tropospheric cooling (Ming et al. 2011; Wang et al. 2016a). For the SH, the subtropical jet in austral winter is weakened by the aerosol-induced interhemispherically asymmetric SST and atmospheric circulation response, while the aerosol-induced subpolar jet response shares similar responses with the GHG forcing with sign reversed (Wang et al. 2020).

Most of the studies introduced above explored the physical mechanisms in understanding the climate response to anthropogenic aerosol forcing by using long-term trends or contrasting two different periods. However, the spatial and temporal changes of anthropogenic aerosols are heterogeneous since the industrial revolution. Understanding the evolving contribution of aerosol and GHG forcing to the historical climate response is of great importance to climate change detection and attribution. In Fig. 1a, the global mean aerosol optical depth (AOD) change shows monotonic increase until the 1990s, and then gradually levels off. Regionally, aerosol emissions in Asia increase consistently until the recent past while EU&NA aerosol emissions reverse in trend before and after the mid-1970s. Spatial patterns of AOD change

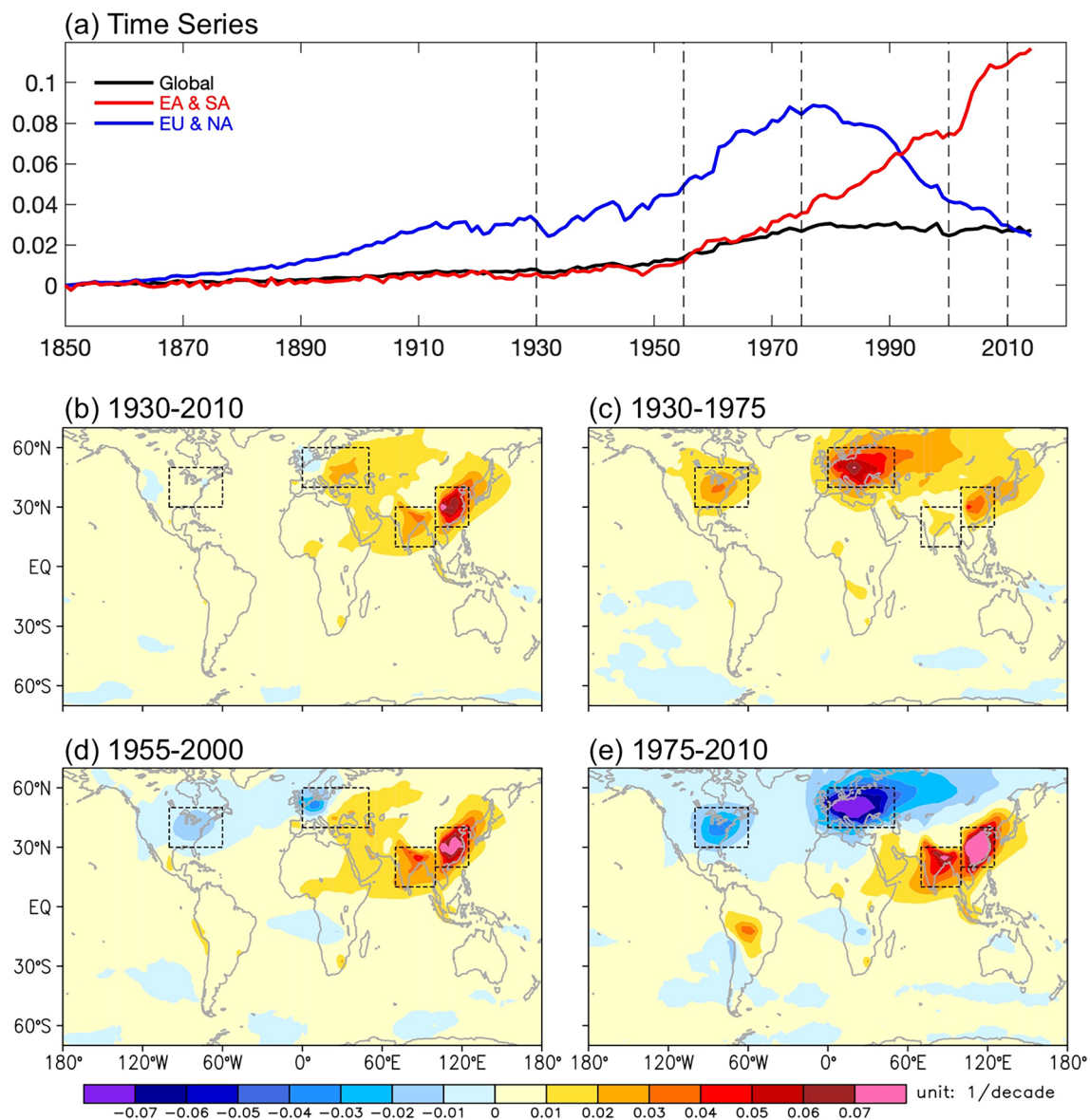


Fig. 1 **a** Global (black line) and regional mean (East Asia (100° E–125° E; 20° N–40° N) and South Asia (70° E–100° E; 10° N–30° N), red line; Europe (0° E–50° E; 40° N–60° N) and North America (100° W–60° W; 30° N–50° N), blue line) Aerosol Optical Depth

(ambient aerosol optical thickness at 550 nm; unit: 1) relative (to year 1850) changes from 1850 to 2020. Aerosol optical depth trend (unit: 1/decade) from **b** 1930–2010, **c** 1930–1975, **d** 1955–2000, **e** 1975–2010

substantially during distinct historical periods (Fig. 1b–e). In 1930–1975, anthropogenic aerosol emissions are concentrated over EU&NA, and to a lesser extent over East and South Asia. In 1955–2000, aerosol emissions shift from the western to the eastern hemisphere, centered over East and South Asia, with little total AOD change over EU&NA. In 1975–2010, a significant seesaw pattern of aerosol emissions emerges, with negative AOD trend over EU&NA but positive AOD trend over East and South Asia. Such spatial and temporal variations of anthropogenic aerosol forcing pose the need to examine their role in regulating the historical climate response, and to evaluate their contribution to the

climate change compared with GHG forcing during these distinct historical periods.

Wang et al. (2015) addressed the emerging issue of the climatic impacts of the west-to-east shift in anthropogenic aerosol emissions with an idealized atmospheric model, focusing on the fast response of the atmospheric system to characteristic aerosol perturbations over the globe. However, our previous studies (Wang et al. 2016a, b) indicated anthropogenic aerosols have a stronger effect on the large-scale circulations through coupled ocean–atmosphere interaction process. Deser et al. (2020) isolated the evolving patterns of precipitation and SST response to aerosol and

GHG forcing with a new set of fully coupled Community Earth System Model version 1 (CESM1) large ensembles (LEs) of simulations. A recent study by Kang et al. (2021) highlighted how the spatial and temporal evolution of AOD in the historical period shaped the large-scale changes in SST and precipitation by idealized experiments with hierarchical models. The aerosol schemes within climate models have undergone significant development in recent years, in particular with regard to the aerosol indirect effect (aerosol–cloud interaction, (Rosenfeld et al. 2008)). More climate models from the latest Coupled Model Intercomparison Project Phase 6 (CMIP6) include representation of aerosol indirect effects which were absent in previous versions. Thus, CMIP6 offers a useful tool to better evaluate the climatic impacts of anthropogenic aerosols. Inspired by these pioneering works, we reveal the climate response to the spatial and temporal changes in anthropogenic aerosols in distinct historical periods with the CMIP6 multi-member and multi-model ensemble mean results. By comparing the aerosol- and GHG-induced climate response patterns, we analyze their climate effect separately and highlight how the patterns of aerosol-forced responses differ from the patterns of GHG-forced responses in shaping the historical climate changes. The focus of this study is on annually averaged changes of SST, precipitation, atmospheric temperature, and

circulation. We aim to extend the understanding of coupled large-scale climate response to anthropogenic aerosol forcing from the long-term change view to a view that includes the spatial and temporal evolutions.

The rest of the paper is organized as follows. Section 2 provides description of the model simulations and analysis methods used in this study. Section 3 investigates the dominant climate response modes to the spatial and temporal evolutions of anthropogenic aerosol forcing. Section 4 describes the evolving contribution of anthropogenic aerosol and GHG forcing to the historical climate response, and further discusses the unique role of anthropogenic aerosol forcing in shaping historical climate change patterns due to distinct forcing spatial patterns in different historical periods. Section 5 is a summary with discussion.

2 Models and methods

We used simulations from the Detection and Attribution Model Intercomparison Project (DAMIP) in the CMIP6 dataset (Table 1; Eyring et al. 2016; Pascoe et al. 2019) to investigate the climate response to the spatial and temporal evolutions of anthropogenic aerosol forcing. We chose thirteen models that performed the historical anthropogenic

Table 1 List of CMIP6 models used in this study

Model acronym	Institution	Ensemble size	
		AOD at 550 nm	Other variables
ACCESS-CM2	Commonwealth Scientific and Industrial Research Organisation (CSIRO), Australian Research Council Centre of Excellence for Climate System Science (ARCCSS), Australia	3	3
ACCESS-ESM1-5	Commonwealth Scientific and Industrial Research Organisation (CSIRO), Australia	3	3
BCC-CSM2-MR	Beijing Climate Center (BCC), China	–	3
CanESM5	Canadian Centre for Climate Modelling and Analysis (CCCma), Canada	15	15
CNRM-CM6-1	Centre National de Recherches Meteorologiques (CNRM), Centre Europeen de Recherche et de Formation Avancee en Calcul Scientifique (CERFACS), France	3	10
FGOALS-g3*	Institute of Atmospheric Physics (IAP), Chinese Academy of Sciences (CAS), China	–	3
GFDL-ESM4*	National Oceanic and Atmospheric Administration, Geophysical Fluid Dynamics Laboratory (NOAA-GFDL), USA	–	1
GISS-E2-1-G	National Aeronautics and Space Administration, Goddard Institute for Space Studies (NASA-GISS), USA	5	5
HadGEM3-GC31-LL	Met Office Hadley Centre (MOHC), UK	4	4
IPSL-CM6A-LR	Institut Pierre Simon Laplace (IPSL), France	10	10
MIROC6	Japan Agency for Marine–Earth Science and Technology (JAMSTEC), Atmosphere and Ocean Research Institute (AORI), National Institute for Environmental Studies (NIES), RIKEN Center for Computational Science (R-CCS), Japan	3	3
MRI-ESM2-0	Meteorological Research Institute (MRI), Japan	5	5
NorESM2-LM*	NorESM Climate modeling Consortium consisting of Center for International Climate and Environmental Research (CICERO), Norwegian Meteorological Institute (MET-Norway), Nansen Environmental and Remote Sensing Center (NERSC), Norwegian	2	3

*Models without surface winds outputs

aerosol/GHG single-forcing simulations (Experiment ID: hist-aer and hist-GHG) and historical all-forcing simulations (Experiment ID: historical) which include both anthropogenic and natural forcings. The AOD at 550 nm was averaged from ten of the thirteen models to evaluate aerosol emissions, and three of the thirteen models did not provide surface winds variables (Table 1). In the single-forcing simulations, the time-evolving changes of anthropogenic aerosol and GHG forced climate responses can help us to reveal their distinct climate response patterns in different historical periods due to these forcings. Comparison between the historical all-forcing and the single-forcing simulations quantifies the relative contribution of an individual radiative forcing to the historical climate change in a specific period. The internal climate variability is important in interpreting the climate response to anthropogenic aerosol forcing for small ensembles (Oudar et al. 2018), which can be evaluated through large ensemble approach (Kay et al. 2015; Oudar et al. 2018; Deser et al. 2020). In this work, to minimize the internal climate variability and the inter-model uncertainty due to different parameterization schemes, we first obtained the multi-member average for each model (ensemble size see Table 1) and then constructed the multi-model ensemble mean results. To facilitate comparison, all the model outputs were interpolated onto a common grid of 144 (zonal) \times 73 (meridional) grid points (2.5° horizontal resolution) with 17 vertical layers from 1000 to 10 hPa.

We focused on the annual mean changes, and a 9-year running average was applied for the time-varying analyses to eliminate the high frequency signal. We performed two kinds of empirical orthogonal function (EOF) analysis on the AOD and aerosol-induced surface temperature (T_{surf}) fields, respectively. The global increase mode of aerosol-induced climate response can be captured by the leading principal component of the traditional EOF analysis after removing the high frequency signal (with 9-year running average). The shift mode of the aerosol-induced climate response was derived from another EOF analysis after the variations at each grid point associated with the global increase mode have been removed through linear regression. We chose the global mean AOD and the aerosol-induced global mean surface temperature (GMST) as the regression indices to eliminate the global increase mode in the original AOD and T_{surf} fields, respectively. The climate response to the spatial and temporal evolutions of aerosol forcing can be captured by regressing the precipitation, surface winds, zonal mean atmospheric temperature and circulation to the leading principal components in the above two EOF analyses.

To further describe the distinct contributions from different spatial patterns of aerosol forcing to the historical climate change, we calculated the trends in three different periods (1930–1975: EU&NA increase; 1955–2000: EU&NA changes little with Asia increase; 1975–2010:

EU&NA decrease with Asia increase) in historical all-forcing and aerosol/GHG single-forcing simulations with Sen's trend (Sen 1968), and assessed the statistical significance at the 90% confidence level using a two-tailed Student's *t* test. Finally, to highlight the distinct patterns of climate response to anthropogenic aerosols versus the GHG-induced changes in different historical periods, we calculated the pattern difference following our previous study (Wang et al. 2016a). We took the GHG-induced climate response as the reference and represent the difference of the aerosol-induced response from the reference as:

$$R_{\text{diff}} = R_{\text{AER}}^* - (-R_{\text{GHG}}^*), \quad (1)$$

where the asterisk denotes the trend normalized by the tropical mean (25° S–25° N) SST change in different historical periods.

3 Aerosol-induced climate response modes

3.1 Global increase mode

As in Fig. 1, the most prominent mode of the AOD change from 1930 to 2010 is the global increase mode, in which anthropogenic aerosols increase most over East and South Asia, and to a lesser extent over EU&NA. We firstly applied an EOF analysis on global AOD and T_{surf} changes during 1930–2010 in historical anthropogenic aerosol single-forcing simulation. Figure 2a shows the leading principal components (PC1) of the EOF analyses on AOD and T_{surf} changes, which explain about 68.9% and 94.8% of the total variance, respectively. With the increasing concentration of anthropogenic aerosols in the NH (Fig. 2b), the T_{surf} shows a prominent interhemispherically asymmetric response pattern with enhanced cooling in the NH relative to the SH (Fig. 2c). Regional features of the aerosol-induced T_{surf} response include the cooling over East and South Asia, EU&NA land regions, which are generated by the “solar dimming” effect from aerosol forcing (Ramanathan et al. 2005). Aerosols from the Eurasia continent are advected by the westerly jet to the adjacent North Pacific, and cool the local SST through both the aerosol-induced radiative flux change at top of the atmosphere and the aerosol–cloud interaction (Wang et al. 2013; Levy et al. 2013; Chen et al. 2016). Over the North Atlantic, an aerosol-induced warming signal due to the Atlantic Meridional Overturning Circulation (AMOC) strengthening (Shi et al. 2018; Hassan et al. 2021) is more pronounced than the cooling signal.

In the regression fields of precipitation and surface winds (Fig. 2d), the decreased rainfall on and north of the equator are regulated by the interhemispheric difference in aerosol-induced SST response, with a significant southward

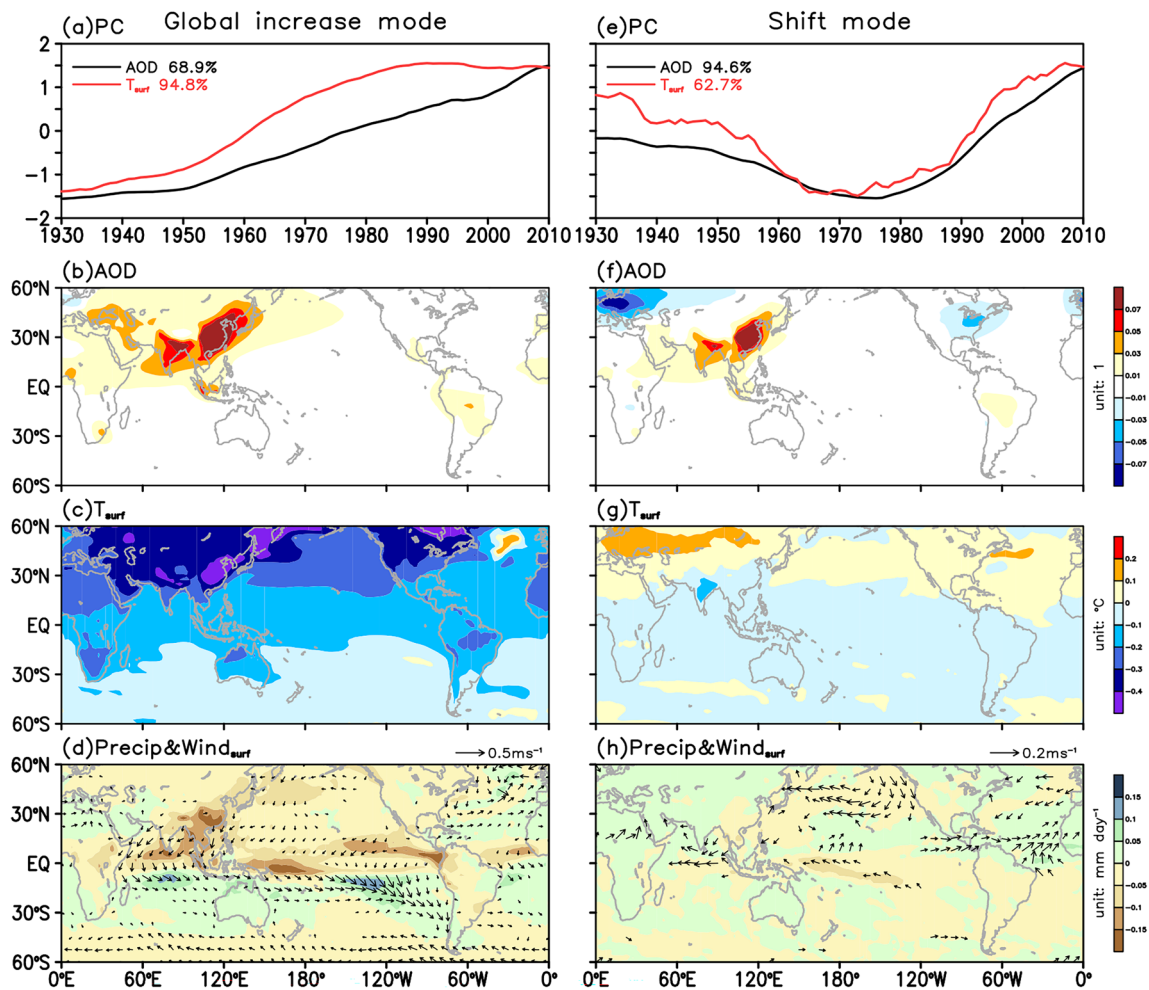


Fig. 2 The increase mode of anthropogenic aerosol-induced climate response derived by the leading EOF modes of AOD (black line in **a** and shading in **b**, unit: 1) and historical anthropogenic aerosol single-forcing induced T_{surf} (red line in **a** and shading in **c**, unit: $^{\circ}\text{C}$), **d** regressions of precipitation (shading; unit: mm day^{-1}) and surface wind (vectors, with scale at top right; wind speed $< 0.02 \text{ m s}^{-1}$ omitted)

ted) to the PC1 of the T_{surf} EOF analysis. The shift mode of anthropogenic aerosol-induced climate response derived by the leading EOF modes after removing the global mean AOD and the aerosol-induced GMST changes (**e–g**), and the regressions of precipitation and surface wind to the derived PC1 of the T_{surf} EOF analysis (**h**). All the time series are normalized by their respective standard deviations

cross-equatorial surface wind change. Over East and South Asian land regions, the Asian monsoon weakening and the drying trends can be either attributed to the atmospheric circulation responses generated by localized emission of anthropogenic aerosols, or due to the large-scale meridional overturning circulation change in response to the interhemispherically asymmetric SST response pattern (Wang et al. 2019; Li et al. 2020). In the Southeastern Pacific, the reduced cooling due to aerosol forcing is associated with weakened southeast trade winds, following the wind-evaporation-SST (WES) feedback (Xie 1996). In the mid- to high-latitude SH, the weakened surface westerlies can be attributed to the barotropic atmospheric circulation change in response to the NH aerosol forcing (Ceppi et al. 2013; Wang et al. 2020).

Besides the surface changes, we also examine the tropospheric temperature and circulation responses in

the aerosol-induced global increase mode by regressing the zonal mean air temperature, zonal wind, and meridional streamfunction to the PC1 of the T_{surf} EOF analysis (Fig. 3a). In the tropics, as pointed out by Xie et al. (2013), the aerosol-induced upward amplified cooling bears some resemblance to the effect of GHG forcing with sign reversed. The unique temperature response induced by aerosol forcing is the deep cooling structure in the NH mid-latitude, which further anchors a westerly acceleration to its south due to thermal wind balance. Regulated by the cross-equatorial energy transport theory (Kang et al. 2008; Chiang and Friedman 2012), an anomalous cross-equatorial overturning circulation is generated in the deep tropics to balance the interhemispheric energy imbalance (Wang et al. 2016a, b), which further regulates the westerly jets response via atmospheric eddy adjustments in

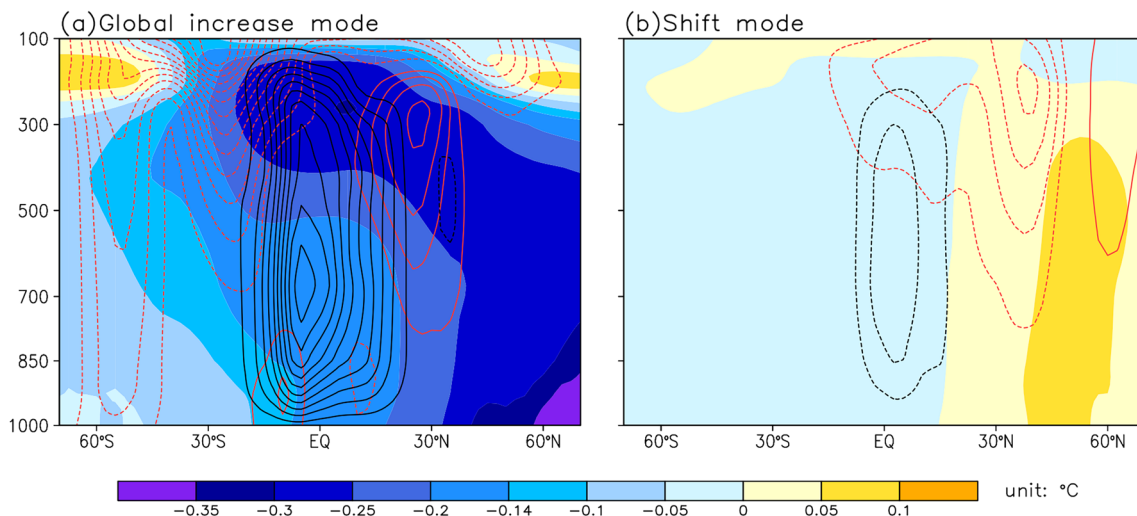


Fig. 3 Regressions of anthropogenic aerosol-induced zonal mean air temperature (shading; unit: °C), meridional streamfunction (black contours at $3 \times 10^6 \text{ kg s}^{-1}$ interval with 0 kg s^{-1} omitted, positive indicates clockwise circulation), and zonal wind speed (red contours at

0.03 m s^{-1} interval with 0 m s^{-1} omitted, positive indicates westerly) to the PC1 (a) and derived PC1 (b) in the aerosol-induced T_{surf} EOF analyses in Fig. 2

both hemispheres (Ceppi et al. 2013; Xu and Xie 2015; Wang et al. 2020).

3.2 Shift mode

The climate effect of the global aerosol emissions increase has been well illustrated by previous studies as well as in the above section. However, with large spatial and temporal changes, the global increase mode cannot completely represent the climate response to anthropogenic aerosol forcing. By regressing out the global increase mode, we derive the shift mode as the other dominant mode of aerosol-induced climate response concerning its spatial and temporal variations during 1930–2010.

After removing the global mean AOD and aerosol-induced GMST changes, the leading modes of the EOF analyses on AOD and T_{surf} present a zonally asymmetric pattern due to the shift of aerosol emissions from the western to the eastern NH before and after the mid-1970s. These modes explain about 94.6% and 62.7% of the total variance for the AOD and T_{surf} respectively (Fig. 2e). The aerosol-induced shift mode is dominated by the aerosol emissions from EU&NA, which increase during 1930–1975 and recover to early twentieth century levels afterwards. The spatial pattern of the T_{surf} response in the aerosol-induced shift mode shows remarkable discrepancies compared with the global increase mode. T_{surf} changes over EU&NA land regions can be attributed to the direct atmospheric response to local aerosol emissions. The downstream effect from the climatological westerlies in the mid-latitude NH generates the local T_{surf} changes via both

radiative effects and aerosol–cloud interaction processes in the North Pacific and the North Atlantic (Fig. 2g). The AMOC response in the shift mode is weaker than that in the global increase mode, indicating the importance of the global cooling in modulating the AMOC changes (Kang et al. 2021). The response of tropical SST is also weak in the shift mode, since the effect of aerosol increase in Asia is partially masked by the decrease from EU&NA. Precipitation and surface wind responses to the shift mode exhibit northward cross-equatorial surface winds over the Pacific and the Atlantic as well as a corresponding northward recovery of the tropical rain-belt (Fig. 2h) due to the interhemispherically asymmetric SST response in contrast to the global increase mode. With the weaker cooling T_{surf} signal in Asian land regions in the shift mode, the Asian monsoon response is relatively weak compared with that in the global increase mode.

In the zonal mean view (Fig. 3b), large tropospheric temperature responses due to the reversing changes of EU&NA aerosol emissions are captured in the NH mid-latitudes. The dominant meridional streamfunction response is similar in pattern to that in the global increase mode with sign reversed, which is the result of the relative SST warming in the North Pacific and the North Atlantic. The zonal mean temperature and circulation changes in the shift mode highlight the importance of the EU&NA aerosol emissions in governing the interhemispheric SST asymmetry and the corresponding tropical atmospheric circulation anomaly through cross-equatorial energy transport.

4 Evolving contributions of aerosol forcing

4.1 Different trends in 3 periods

To better describe the evolving climate response to the distinct anthropogenic aerosol forcing spatial patterns, and weight their evolving contributions to the historical climate change, we present the T_{surf} , precipitation, surface winds, atmospheric temperature and circulation changes in historical all-forcing and single-forcing simulations based on the multi-member and multi-model ensemble mean trends for three overlapping periods as defined in Sect. 2.

In the historical all-forcing simulations, the North–South interhemispherically asymmetric T_{surf} response during 1930–1975 is dominated by the aerosol emissions from EU&NA, with the largest cooling over EU&NA land regions as well as over the North Pacific and the North Atlantic (Fig. 4a). During 1955–2000, T_{surf} trends in historical all-forcing simulations are positive over most of the globe except for the East and South Asia land regions, a result of the joint effect of GHG-induced warming and cooling from East and South Asian aerosol emissions (Fig. 4b). In the third period 1975–2000, the GHG forcing dominates the T_{surf} change globally, and the maximum warming signals over Eurasia and NA are amplified by the declining local aerosol emissions (Fig. 4c).

The T_{surf} responses over land in historical anthropogenic aerosol single-forcing simulations closely resembles the AOD change in all three periods (Fig. 4d–f). Globally, spatial correlations of T_{surf} trends between all-forcing and aerosol single-forcing simulations declines from 0.83 in the first period to 0.39 in the third period, indicating the gradually weakened contribution from aerosol forcing to the historical T_{surf} response patterns. Remarkably, the SST changes in aerosol single-forcing simulations show quite distinct spatial patterns in the different periods. During 1930–1975, the SST cooling is centered in the North Pacific and the North Atlantic due to EU&NA aerosol emissions. In the second period, when total EU&NA aerosol emissions trends are small, the aerosol forcing from increasing Asian aerosol emissions cannot generate significant SST cooling in the North Pacific as in the first period. This suggests that the aerosols advected from northern Eurasia in the first period is far more effective in perturbing the North Pacific SST than the local aerosol increase over the low-latitude Asian region. The equatorial symmetric SST cooling structure is more obvious in this period. Previous studies demonstrated that such a La Nina like SST cooling can be attributed to the extratropical cooling in either hemisphere via ocean circulation adjustments (Kang et al. 2020). In the third period, with the cancellation effect of aerosol emissions between EU&NA and Asia, the SST changes over the globe are weak except for that in the subpolar north Atlantic, which may be associated with

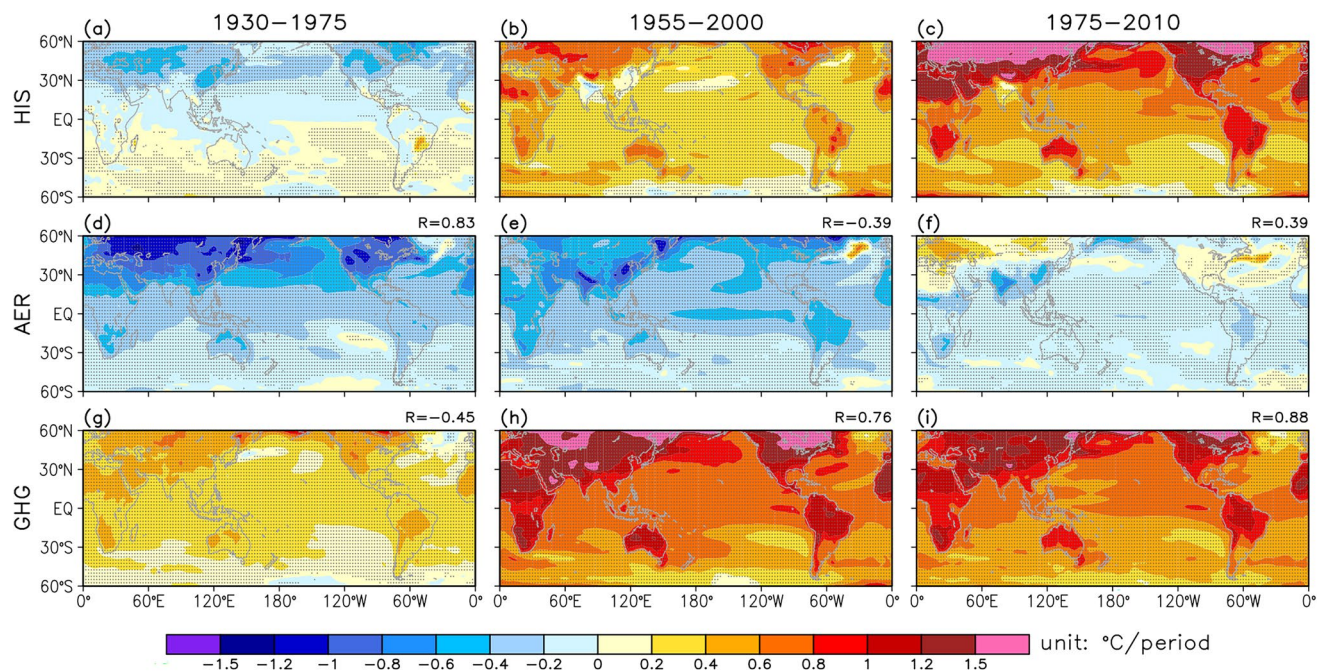


Fig. 4 Trends of surface temperature (unit: °C per period) in historical all-forcing (HIS, first row), historical anthropogenic aerosol single-forcing (AER, second row), and historical greenhouse gas single-forcing (GHG, third row) during 1930–1975 (first column),

1955–2000 (second column), and 1975–2010 (third column). Spatial correlations between the single-forcing results and the all-forcing results are marked on top right in each panel. Stippled regions indicate changes exceed 90% statistical confidence

the AMOC response to the global cooling (Shi et al. 2018; Menary et al. 2020; Hassan et al. 2021). The dynamics of the SST response patterns in aerosol single-forcing simulations across different periods require further investigations concerning the role of ocean dynamical and coupled ocean–atmosphere interaction processes.

In GHG single-forcing simulations, the spatial pattern of T_{surf} response is static, with increasing magnitude due to the growth of GHG emission (Fig. 4g–i). The increasing resemblance between all-forcing and GHG single-forcing simulations is evident, with the spatial pattern correlation increases from -0.45 in the first period to 0.88 in the third period. The warming pattern includes the larger response over land than ocean, and the SST spatial pattern is in consistent with previous studies (Xie et al. 2010).

Mediated by the “warmer-get-wetter” mechanism (Xie et al. 2010), the tropical precipitation response follows the evolution of SST spatial patterns in different simulations. In historical all-forcing simulations, the tropical rainfall changes markedly from an interhemispherically asymmetric pattern in the first period to an equatorial symmetric pattern in the third period (Fig. 5a–c). During 1930–1975, the ITCZ is shifted southward accompanying the southward cross-equatorial surface wind anomalies in response to the interhemispheric SST difference. In the second period, weakened rainfall response in the equatorial Pacific can be attributed to the cancellation effect of the aerosol- and GHG- induced

SST responses. With the increasing contribution from GHG forcing, an intensification of the ITCZ is seen in the third period, with surface winds enhancing the rainfall through the WES feedback (Xie 1996) in the eastern equatorial Pacific. It is worth noticing that in the Atlantic sector during 1975–2010, the northward recovery of tropical rain-belt and the northward cross-equatorial winds in the historical all-forcing simulation are caused by the declining aerosol emissions from EU&NA.

Anthropogenic aerosol-induced tropical precipitation trends show robust decrease on and north of the equator but increase to the south, along with southward cross-equatorial wind anomalies in all three basins during 1930–1975 (Fig. 5d). The spatial correlation of tropical (30°S – 30°N) precipitation between the all-forcing and aerosol single-forcing simulations in the first period is 0.61 , indicating the important role of aerosol-induced interhemispheric SST difference in regulating the tropical rainfall response in historical climate change. During 1955–2000, with the aerosol forcing mainly originated from the Asian emissions, the spatial correlation of tropical rainfall between aerosol single-forcing and all-forcing is 0.23 . In contrast to the interhemispherically asymmetric rainfall response pattern in the first period, there is a large degree of equatorially symmetric rainfall decrease in the tropics in the second period (Fig. 5e), similar to that in the SST response (Fig. 4e). This unique feature is probably due to the altered distribution of aerosol

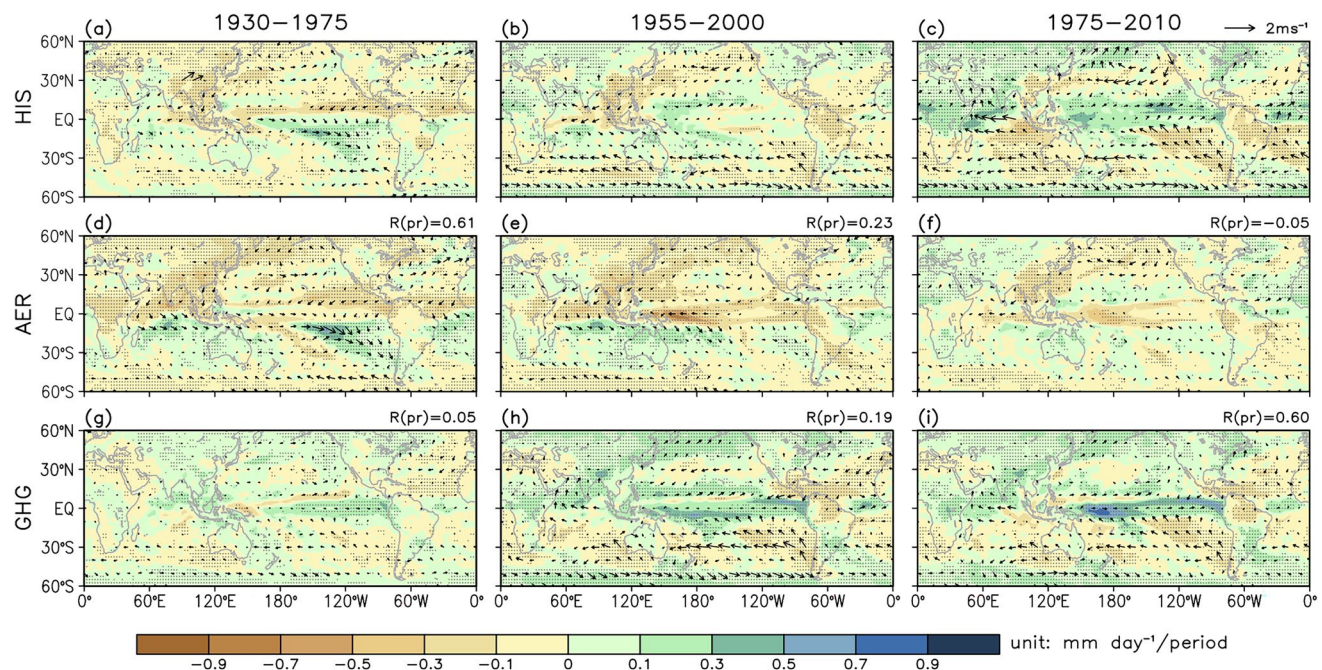


Fig. 5 As in Fig. 4 but for changes in tropical precipitation (shading, unit: mm day⁻¹ per period) and surface wind (vectors, with scale at top right; wind speed <0.03 m s⁻¹ per period omitted). Spatial correlations of tropical (30°S – 30°N) precipitation trends between the sin-

gle-forcing results and the all-forcing results are marked on top right in each panel. Stippled regions indicate precipitation changes exceed 90% statistical confidence

emissions from the mid-latitude EU&NA to the low-latitude Asia. The effect of aerosol forcing in the low-latitudes resembles the way the GHG forcing affects the tropical climate response with sign reversed (Xie et al. 2013). In the third period, this spatial correlation is as low as -0.05 , and the aerosol-induced rainfall change only contributing to the Atlantic tropical rainfall response in historical all-forcing simulations (Fig. 5f). Rainfall change in response to aerosol forcing during 1975–2010 shows meridionally symmetric but zonally asymmetric pattern over the Pacific, decreasing more in the equatorial western Pacific than that in the equatorial eastern Pacific. Surface wind changes follow the rainfall anomaly in the equatorial Pacific and Indian Ocean, hinting at an intensification of the Walker circulation.

Similar to the SST trends evolutions, the GHG-induced tropical precipitation trends are spatially consistent with increasing magnitude from the first to the third period (Fig. 5g–i). Along with the relative warming on the equator, GHG forcing induces the rainfall increase over the equatorial Pacific and Atlantic, with compensating rainfall decrease off the equator. Due to the relatively uniform SST warming, spatial patterns of precipitation changes in the tropical Indian Ocean are weak compared with that in the tropical Pacific and Atlantic, which were mediated by the “warmer-get-wetter” mechanism (Xie et al. 2010). The spatial correlations between all-forcing and GHG single-forcing changes from 0.05 in the first period to 0.60 in the third period, indicating the increasing contribution from GHG forcing to the historical tropical precipitation change.

The evolving trends of zonal mean atmospheric temperature, zonal wind, and meridional streamfunction in all-forcing and single-forcing simulations are shown in Fig. 6. It shows a north-cooling/south-warming pattern in the first period, following with a relatively equatorial symmetric warming pattern in the latter half of the twentieth century, and ending with a NH warmer pattern during 1975–2010 (Fig. 6a–c). In aerosol runs, the prominent temperature response in the first period is the atmospheric cooling over the NH mid-latitude as shown with the aerosol-induced global increase mode (Fig. 6d). In the second period, the temperature response generated by the increasing Asian aerosol emissions resembles that in the GHG runs with sign reversed, echoing the SST and precipitation changes (Fig. 6e). Due to the cancellation effect of the aerosol emissions from Asia and EU&NA, the temperature response is weak in the third period with some warming in the NH mid-to high-latitudes (Fig. 6f). Temperature changes in GHG runs in all three periods show equatorial symmetric patterns with upper troposphere amplified warming (Santer et al. 2005). The warming amplitude increases with the increasing concentration of GHG from the first to the third period (Fig. 8g–i). The meridional streamfunction changes (black contours in Fig. 6) which balance the interhemispheric

energy imbalance in the atmosphere are sensitive to the interhemispheric thermal contrast. A significant clockwise cross-equatorial anomalous Hadley cell can be seen in the first period in the historical all-forcing simulations, which is dominated by the anthropogenic aerosol forcing (Fig. 6a, d). In the second period, the streamfunction trends are relatively weak and symmetric about the equator (Fig. 6b). In the third period, the amplified warming in the NH mid- to high-latitudes in the all-forcing runs is dominated by the aerosol- and GHG-induced warming jointly (Fig. 6c, f, i), which generates an anticlockwise cross-equatorial circulation anomaly (Fig. 6c). The spatial correlation of the meridional streamfunction trends between aerosol forcing and all-forcing is highest in the first period (0.97), and gradually decreases over time (0.28 in the second period; 0.17 in the third period). On the contrary, spatial correlation between GHG forcing and all-forcing rises from -0.14 in the first period to 0.58 in the second period, and up to 0.87 in the third period. Zonal wind changes (grey contours in Fig. 6) are regulated by the thermal wind balance and the geostrophic effect related to the temperature and meridional overturning circulation trends, respectively.

4.2 Distinctive patterns in 3 periods

The above analyses based on the single forcing simulations determined the temporal climate responses to different forcings. Furthermore, the pattern differences between aerosol- and GHG-induced responses (R_{diff}) have been demonstrated to be a useful metric to isolate the unique role of anthropogenic aerosol forcing in shaping the historical climate change in comparison with GHG forcing (Wang et al. 2016a).

Results in Fig. 7 show the zonal mean atmospheric temperature and circulation pattern differences between aerosol and GHG forcing. In the first period, the aerosol-induced interhemispherically asymmetric response pattern is the main pattern difference between aerosol and GHG responses, featuring tropospheric cooling centered around 40° N and a corresponding southward shift of the NH westerly jet as well as a clockwise cross-equatorial anomalous Hadley cell in the tropics (Fig. 7a). In the second period, as the aerosol forcing shifts from the mid-latitude EU&NA to the low-latitude Asian regions, the tropospheric interhemispheric temperature contrast is relatively weak. However, the aerosol-induced near surface cooling in the NH also generates a clockwise cross-equatorial anomalous Hadley cell in the tropics, though with weaker magnitude than the first period (Fig. 7b). In the third period, warming in the NH mid-to high-latitude induced by the declining aerosol emissions from EU&NA and the GHG forcing creates a north-warmer interhemispheric thermal contrast, which further induces an

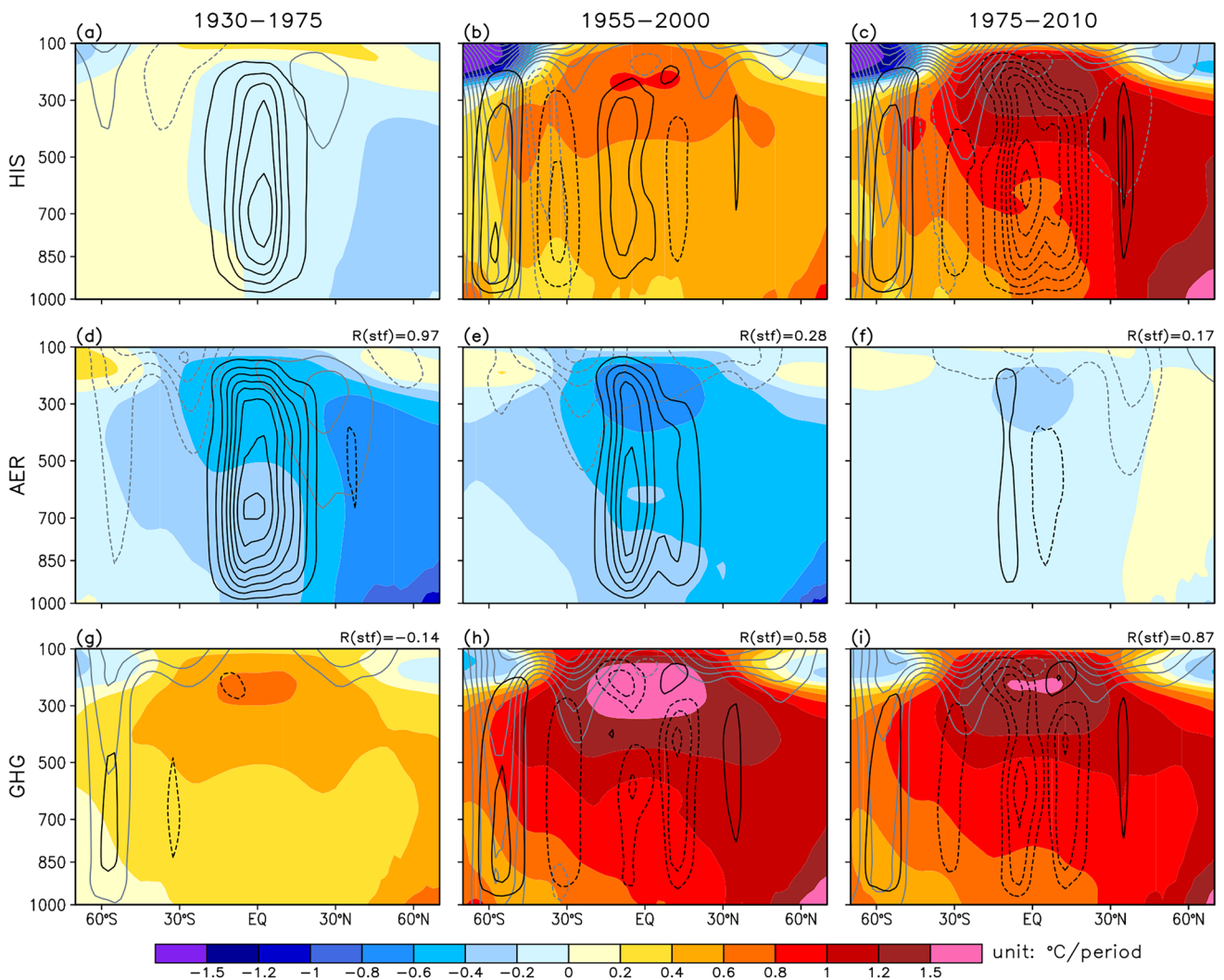


Fig. 6 As in Fig. 4 but for changes in zonal mean air temperature (shading, unit: $^{\circ}\text{C}$ per period), meridional streamfunction (black contours at $1 \times 10^7 \text{ kg s}^{-1}$ per period interval with 0 kg s^{-1} per period omitted, positive indicates clockwise circulation), and zonal wind

speed (grey contours at 0.2 m s^{-1} per period interval with 0 m s^{-1} per period omitted, positive indicates westerly). Spatial correlations of meridional streamfunction trends between the single-forcing results and the all-forcing results are marked on top right in each panel

anticlockwise Hadley circulation anomaly over the equator (Fig. 7c).

The anomalous interhemispheric thermal contrast and circulation changes in different historical periods are associated with the zonal mean SST and precipitation changes. The radiative difference between the NH and the SH requires the anomalous cross-equatorial Hadley circulation to compensate the interhemispheric energy imbalance, though this energy theory applies only to the zonal mean (Kang et al. 2008; Chiang and Friedman 2012; Frierson and Hwang 2012; Hwang et al. 2013; Wang et al. 2016b). In the view of energy conservation theory, the zonal mean SST and precipitation R_{diff} further isolate and highlight the role of anthropogenic aerosol forcing in shaping the historical climate change in comparison with GHG forcing. The zonal mean

SST R_{diff} patterns in all the three periods are regulated by the distinct spatial patterns of aerosol forcing (Fig. 8a). The zonal mean precipitation change is a surface manifestation of the anomalous Hadley circulation, with southward shift of the ITCZ in the first period; negative equatorial peak in the second period; northward recovery of the ITCZ in the third period (Fig. 8b).

Spatial patterns of R_{diff} further characterize the distinct regional climate responses induced by aerosol and GHG forcings in different historical periods. For the SST changes, remarkable cooling induced by the aerosol forcing relative to GHG appears in the North Pacific in the early period (Fig. 9a). Afterwards in the second period, the effect of aerosol increase over Asia on SST response is restricted in the equatorial Pacific (Fig. 9b). In the third period, the

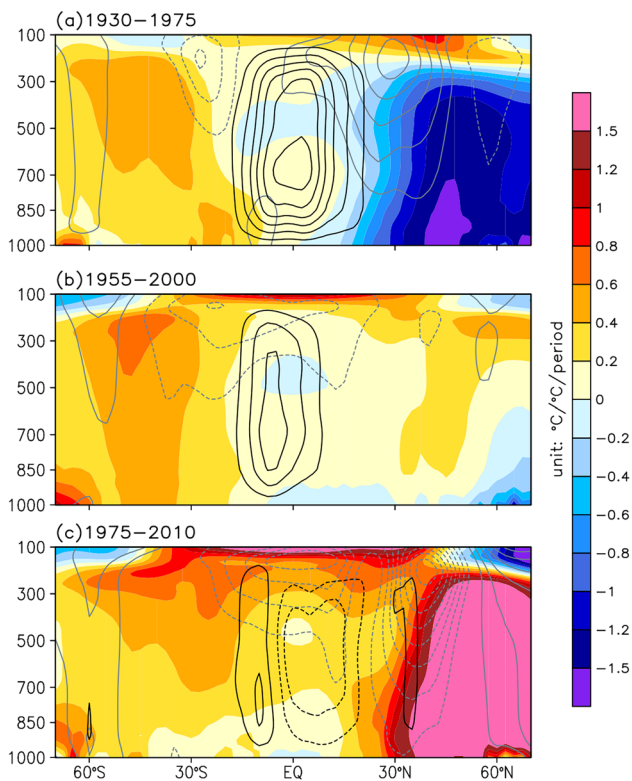


Fig. 7 Difference in climate response pattern between anthropogenic aerosol and greenhouse gas single-forcing [defined in Eq. (1)] in zonal mean air temperature (shading, unit: $^{\circ}\text{C}/^{\circ}\text{C}$ per period), meridional streamfunction (black contours at $5 \times 10^7 \text{ kg s}^{-1}/^{\circ}\text{C}$ per period interval with $0 \text{ kg s}^{-1}/^{\circ}\text{C}$ per period omitted, positive indicates clockwise circulation), and zonal wind speed (grey contours at $0.5 \text{ m s}^{-1}/^{\circ}\text{C}$ per period interval with $0 \text{ m s}^{-1}/^{\circ}\text{C}$ per period omitted, positive indicates westerly) during **a** 1930–1975, **b** 1955–2000, **c** 1975–2010

SST cooling over the equatorial Pacific, the low-latitude Northwestern Pacific, and the North Indian Ocean are generated by the dramatic increase in aerosol emissions over Asia (Fig. 9c). In the mid-latitude, the GHG forcing and the declining aerosol emissions from EU&NA lead to the anomalous SST warming over the North Pacific and the North Atlantic. Corresponding to the SST patterns, the southward shift of tropical rain-belt can be seen in all the three tropical basins in the first period, along with the southward cross-equatorial wind responses due to the aerosol forcing (Fig. 9d). In the second and third periods, the tropical rainfall and surface winds responses are more symmetric about the equator, with rainfall decrease in the equatorial Pacific, indicating the aerosol cooling is much more efficient in generating the tropical rainfall response than the GHG warming (Fig. 9e). The aerosol forcing also generates a northward recovery of the tropical rainfall in the Atlantic and Sahel (Fig. 9f) due to the reduction of aerosol emissions over EU&NA in the third period. The patterns differences clearly quantify the relative efficiency of aerosol and GHG forcing in generating the historical climate changes in different historical periods, highlighting the distinct spatial and temporal climate response patterns induced by aerosol forcing in comparison with GHG forcing.

5 Summary and discussion

Anthropogenic aerosols, as one of the major drivers of climate change, have significantly modulated the climate response since the industrial revolution. Due to the heterogeneous emission sources and short atmospheric resident time, the role of the spatial and temporal changes of anthropogenic aerosol forcing in modulating the historical

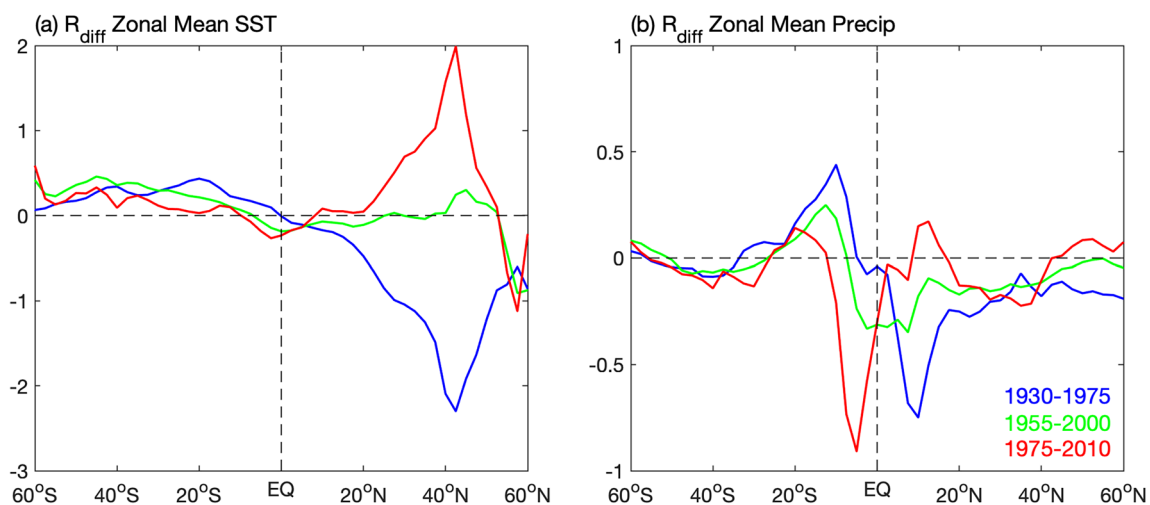


Fig. 8 As in Fig. 7 but for **a** zonal mean SST changes (unit: $^{\circ}\text{C}/^{\circ}\text{C}$ per period), and **b** zonal mean precipitation (unit: $\text{mm day}^{-1}/^{\circ}\text{C}$ per period) changes

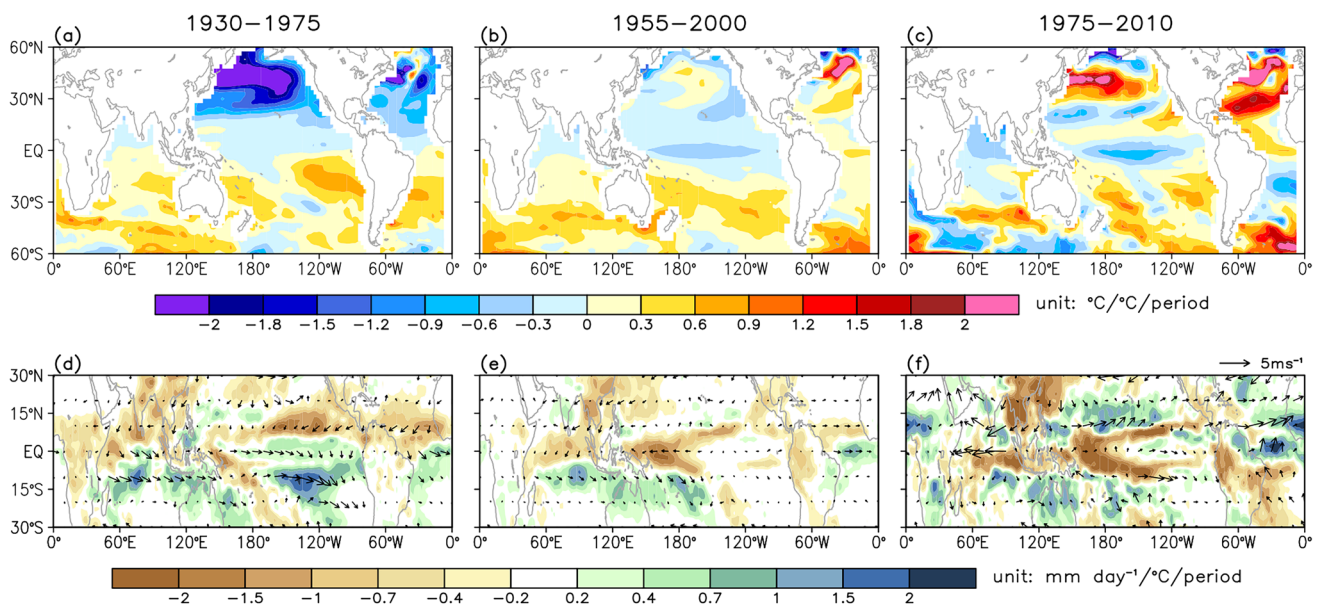


Fig. 9 As in Fig. 7 but for **a–c** SST changes (shading, unit: $^{\circ}\text{C}/^{\circ}\text{C}$ per period), and **d–f** precipitation (shading, unit: $\text{mm day}^{-1}/^{\circ}\text{C}$ per period) and surface wind (vectors, with scale at bottom right; wind speed $< 0.03 \text{ m s}^{-1}/^{\circ}\text{C}$ per period omitted) changes

climate response has drawn much attention recently (Wang et al. 2015; Samset et al. 2019; Deser et al. 2020; Wilcox et al. 2020; Qin et al. 2020; Kang et al. 2021). Here, we focus on the spatial and temporal evolutions of anthropogenic aerosol forcing and reveal their role in shaping the historical climate change since the industrial revolution, extending our previous understandings of the aerosol effect on climate system.

Over the globe, anthropogenic aerosol emissions increase since the industrial revolution until the 1990s, which generates the global increase mode to the first order. The global increase in anthropogenic aerosol emissions leads to the interhemispherically asymmetric temperature and atmospheric circulation responses regulated by the cross-equatorial energy transport theory, featuring the southward shift of the ITCZ, southward cross-equatorial surface wind anomalies, as well as the mid-latitude jet responses in both hemispheres. In addition to the global increase mode, regional aerosol emissions show large spatial variations in distinct historical periods. After removing the global increase mode, we obtain the second dominant climate mode (shift mode) in response to aerosol forcing, which is generated by the reversal of aerosol emissions trends over the EU&NA before and after the mid 1970s. The shift mode not only features the regional responses over the North Atlantic and Sahel, but also the anomalous anticlockwise Hadley circulation anomaly and the corresponding northward recovery of the tropical rain-belt, indicating the important role of the EU&NA aerosol forcing in modulating the interhemispheric thermal contrast.

More systematically, we separate the aerosol-induced historical climate response into three overlapping periods to describe the evolving contributions from distinct aerosol forcing spatial patterns to the historical climate changes. In the first period (1930–1975), the anthropogenic aerosol increased most over the EU&NA, and to a lesser extent over the Asian regions. The climate response in this period is similar to that in the global increase mode. In the second period (1955–2000), anthropogenic aerosol emissions over Asia increased significantly while there is little change in aerosol emissions over the EU&NA. The aerosol-induced radiative forcing shifts from the NH mid-latitudes to the low-latitudes, inducing distinct climate response pattern compared with the first period, featuring significant equatorial symmetric SST cooling in the tropical Pacific. This indicates that the radiative forcing change induced by the aerosol emissions over the EU&NA is more effective in generating the interhemispheric thermal contrast compared with the Asian aerosol forcing. In the third period (1975–2010), Asian aerosol emissions increase rapidly while the EU&NA aerosol emissions decline to their early twentieth century levels. The net radiative forcing change in the NH during this period is small and the dipole pattern of aerosol forcing only mediates the regional T_{surf} response over the EU&NA and the Asian land regions. The localized aerosol effects are also seen in a weakened Asian summer monsoon and the recovery of Sahel rainfall in this period.

As the high-latitude radiative forcing is more effective in driving the temperature response than the low-latitude radiative forcing (Seo et al. 2014; Kang et al. 2017), the

aerosol-induced large-scale climate response shifts from an interhemispherically asymmetric pattern to an equatorial symmetric and more localized pattern from 1930 to 2010. With the increasing strength of the GHG forcing, the relative importance of aerosol and GHG forcing in shaping the historical climate response pattern has shifted from the aerosol-dominant to the GHG-dominant over time. Although the robust warming induced by GHG forcing masked the aerosol-induced cooling signal in the latter half of the twentieth century. The pattern difference analyses between aerosol and GHG runs isolate the distinct climate response patterns induced by aerosol forcing, and highlight the high relative efficiency of anthropogenic aerosol forcing in shaping the regional climate changes in comparison with GHG forcing.

Our findings are based on the multi-member and multi-model ensemble mean results in CMIP6. However, anthropogenic aerosols are the largest source of uncertainty in radiative forcing during the instrumental era because of insufficient understanding of aerosol microphysical effects on cloud and precipitation (Boucher et al. 2013). Even though the changes in precipitation and SST in the ensemble mean are robust, their inter-model standard deviations are substantial in both the historical all-forcing and single-forcing simulations (Fig. 10). According to the cross-equatorial energy transport theory, large uncertainty in tropical rainfall response may be attributed to the uncertainty in interhemispheric thermal contrast which is due to the

uncertainty in the mid- to high-latitude SST responses. Inter-model uncertainties in aerosol forcing magnitude and pattern which are related to the model parameterizations may be the basis of much of the uncertainties in SST responses. In addition, similar patterns of inter-model uncertainties in precipitation responses between aerosol and GHG forcings indicate that much of the uncertainties might not be specifically related to the specific character of each forcing. The model uncertainty analyses are beyond the scope of this work and call for further investigations in interpreting the climate response to the spatial and temporal variations of anthropogenic aerosol forcing.

Our results regarding the distinct climate responses in different historical periods were based on the AOD changes in CMIP6 climate models, which may have discrepancies from other climate model results and the observations (Deser et al. 2020). The single forcing simulations can help to distinguish the aerosol effect on historical climate change and an index that can be applied to the observations is needed in future studies. As regional aerosol emissions are rapidly changing, a dipole forcing pattern is seen between the South and East Asia since 2010 due to the Clean Air Action in China (Zheng et al. 2018; Samset et al. 2019). It will be important to put our effort into understanding and quantifying the impact of this emerging Asian aerosol patterns on both the regional and hemispheric climate responses in the near future.

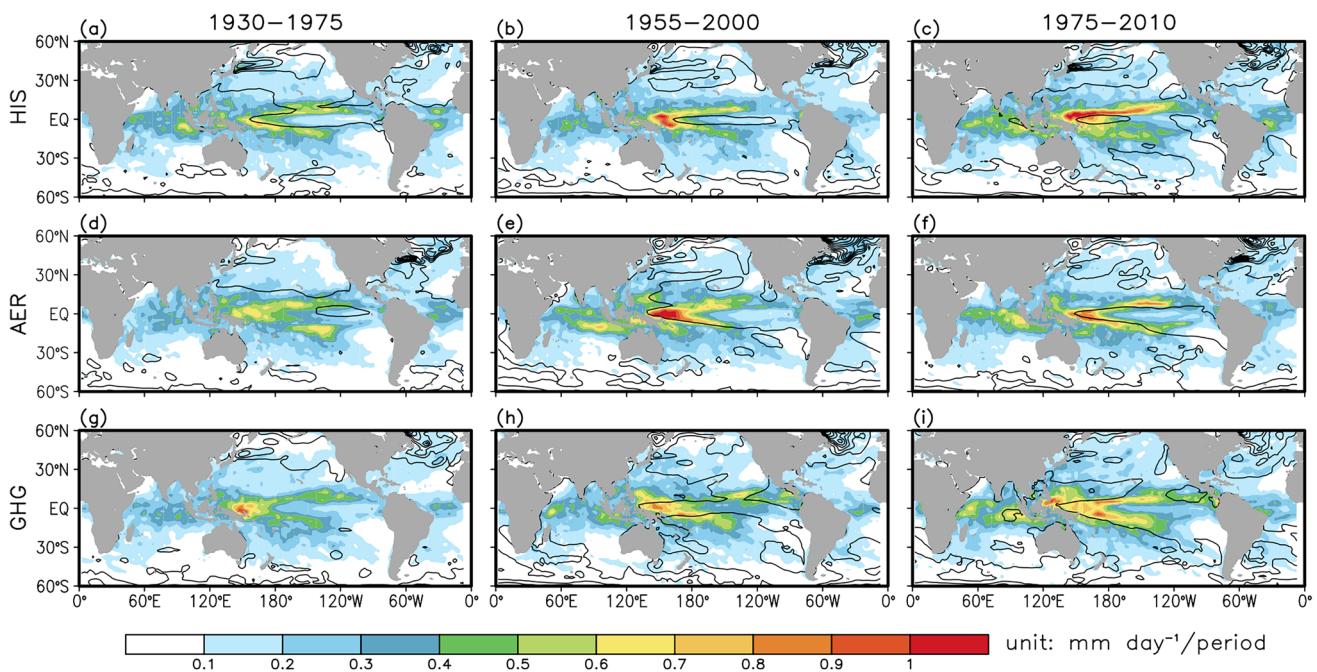


Fig. 10 Inter-model standard deviations of precipitation (shading, unit: mm day^{-1} per period) and SST (contours at $0.2\text{ }^{\circ}\text{C}$ per period interval) responses in historical all-forcing (HIS, first row), historical anthropogenic aerosol single-forcing (AER, second row), and his-

torical greenhouse gas single-forcing (GHG, third row) during 1930–1975 (first column), 1955–2000 (second column), and 1975–2010 (third column)

Acknowledgements This work was supported by the National Key Research and Development Program of China (2018YFA0605704), and the National Natural Science Foundation of China (41806006, 41975092, 42011540386). We acknowledge the World Climate Research Programme Working Group on Coupled Modeling, which is responsible for CMIP6, and the climate modeling groups (Table 1) for producing and making available their model outputs. All the CMIP6 data were downloaded from <https://esgf-node.llnl.gov/search/cmip6/>. We thank the two anonymous reviewers for their useful comments and suggestions.

Funding This work was supported by the National Key Research and Development Program of China (2018YFA0605704), and the National Natural Science Foundation of China (41806006, 41975092, 42011540386).

Data availability The simulations are part of the Detection and Attribution Model Intercomparison Project (DAMIP) in the Phase 6 of Coupled Model Intercomparison Project (CMIP6) and model simulation outputs can be obtained via the Earth System Grid Federation (ESGF) nodes, <https://esgf-node.llnl.gov/search/cmip6/>.

Code availability Scripts for analyzing the data will be available from the corresponding author upon reasonable request.

Declarations

Conflict of interest The authors have no competing interests to declare that are relevant to the content of this article.

References

- Albrecht BA (1989) Aerosols, cloud microphysics, and fractional cloudiness. *Science* 245:1227–1230. <https://doi.org/10.1126/science.245.4923.1227>
- Allen RJ, Evan AT, Booth BBB (2015) Interhemispheric aerosol radiative forcing and tropical precipitation shifts during the late twentieth century. *J Clim* 28(20):8219–8246. <https://doi.org/10.1175/JCLI-D-15-0148.1>
- Bellouin N et al (2020) Bounding global aerosol radiative forcing of climate change. *Rev Geophys*. <https://doi.org/10.1029/2019RG000660>
- Boer G, Yu B (2003) Climate sensitive and response. *Clim Dyn* 20(4):415–429. <https://doi.org/10.1007/s00382-002-0283-3>
- Bollasina MA, Ming Y, Ramaswamy V (2011) Anthropogenic aerosols and the weakening of the South Asian summer monsoon. *Science* 334(6055):502–505. <https://doi.org/10.1126/science.1204994>
- Bollasina MA, Ming Y, Ramaswamy V (2013) Earlier onset of the Indian monsoon in the late twentieth century: the role of anthropogenic aerosols. *Geophys Res Lett* 40:3715–3720. <https://doi.org/10.1002/grl.50719>
- Booth BBB, Dunstone NJ, Halloran PR, Andrews T, Bellouin N (2012) Aerosols implicated as a prime driver of twentieth-century North Atlantic climate variability. *Nature* 484(7393):228–232. <https://doi.org/10.1038/nature10946>
- Boucher O et al (2013) Clouds and aerosols. In: Stocker TF et al (eds) *Climate change 2013: the physical science basis*. Cambridge University Press, Cambridge, pp 571–657
- Ceppi P, Hwang YT, Liu X, Frierson DMW, Hartmann D (2013) The relationship between the ITCZ and the Southern Hemispheric eddy-driven jet. *J Geophys Res Atmos* 118(11):5136–5146. <https://doi.org/10.1002/jgrd.50461>
- Chen JP, Chen JJ, Tsai IC (2016) Dynamic feedback of aerosol effects on the East Asian summer monsoon. *J Clim* 29:6137–6149. <https://doi.org/10.1175/JCLI-D-15-0758.1>
- Chiang JCH, Friedman AR (2012) Extratropical cooling, interhemispheric thermal gradients, and tropical climate change. *Annu Rev Earth Planet Sci*. <https://doi.org/10.1146/annurev-earth-042711-105545>
- Deser C et al (2020) Isolating the evolving contributions of anthropogenic aerosols and greenhouse gases: a new CESM1 large ensemble community resource. *J Clim* 33(18):7835–7858. <https://doi.org/10.1175/JCLI-D-20-0123.1>
- Dong B, Sutton R (2015) Dominant role of greenhouse-gas forcing in the recovery of Sahel rainfall. *Nat Clim Change* 5(8):757–760. <https://doi.org/10.1038/nclimate2664>
- Dong B, Sutton R, Highwood E, Wilcox L (2014) The impacts of European and Asian anthropogenic sulphur dioxide emissions on Sahel rainfall. *J Clim* 27(18):7000–7017. <https://doi.org/10.1175/JCLI-D-13-00769.1>
- Eyring V, Bony S, Meehl GA, Senior CA, Stevens B, Stouffer RJ, Taylor KE (2016) Overview of the Coupled Model Intercomparison Project Phase 6 (CMIP6) experimental design and organization. *Geosci Model Dev* 9(5):1937–1958. <https://doi.org/10.5194/gmd-9-1937-2016>
- Forster P et al (2007) Changes in atmospheric constituents and in radiative forcing. In: Stocker S et al (eds) *Climate change 2007: the physical science basis*. Cambridge University Press, Cambridge, pp 129–234
- Frierson DMW, Hwang YT (2012) Extratropical influence on ITCZ shifts in slab ocean simulations of global warming. *J Clim* 25:720–733. <https://doi.org/10.1175/JCLI-D-11-00116.1>
- Ganguly D, Rasch PJ, Wang H, Yoon JH (2012) Fast and slow responses of the South Asian monsoon system to anthropogenic aerosols. *Geophys Res Lett* 39(18):L18804. <https://doi.org/10.1029/2012GL053043>
- Giannini A, Kaplan A (2019) The role of aerosols and greenhouse gases in Sahel drought and recovery. *Clim Change* 152(3–4):449–466. <https://doi.org/10.1007/s10584-018-2341-9>
- Hassan T, Allen RJ, Liu W, Randles CA (2021) Anthropogenic aerosol forcing of the Atlantic meridional overturning circulation and the associated mechanisms in CMIP6 models. *Atmos Chem Phys* 21(8):5821–5846. <https://doi.org/10.5194/acp-21-5821-2021>
- Haywood JM, Jones A, Bellouin N, Stephenson D (2013) Asymmetric forcing from stratospheric aerosols impacts Sahelian rainfall. *Nat Clim Change* 3:660–655. <https://doi.org/10.1038/nclimate1857>
- Held IM, Soden BJ (2006) Robust responses of the hydrological cycle to global warming. *J Clim* 19:5686–5699. <https://doi.org/10.1175/JCLI3990.1>
- Hirasawa H, Kushner PJ, Sigmund M, Fyfe J, Deser C (2020) Anthropogenic aerosols dominate forced multidecadal Sahel precipitation change through distinct atmospheric and oceanic drivers. *J Clim* 33(23):10187–10204. <https://doi.org/10.1175/JCLI-D-19-0829.1>
- Huang P, Xie SP, Hu K, Huang G, Huang R (2013) Patterns of the seasonal response of tropical rainfall to global warming. *Nat Geosci* 6(5):357–361. <https://doi.org/10.1038/ngeo1792>
- Hwang YT, Frierson DMW, Kang SM (2013) Anthropogenic sulfate aerosol and the southward shift of tropical precipitation in the late 20th century. *Geophys Res Lett* 40:2845–2850. <https://doi.org/10.1002/grl.50502>
- Kang SM, Held IM, Frierson DMW, Zhao M (2008) The response of the ITCZ to extratropical thermal forcing: idealized slab-ocean experiments with a GCM. *J Clim* 21(14):3521–3532. <https://doi.org/10.1175/2007JCLI1246.1>
- Kang SM, Park K, Jin FF, Stuecker MF (2017) Common warming pattern emerges irrespective of forcing location. *J Adv Model*

- Earth Syst 9(6):2413–2424. <https://doi.org/10.1002/2017M5001083>
- Kang SM, Xie SP, Shin Y, Kim H, Hwang YT, Stuecker MF, Xiang B, Hawcroft M (2020) Walker circulation response to extratropical radiative forcing. *Sci Adv* 6(47):eabd3021. <https://doi.org/10.1126/aciadv.abd3021>
- Kang SM, Xie SP, Deser C, Xiang B (2021) Zonal mean and shift modes of historical climate response to evolving aerosol distribution. *Sci Bull*. <https://doi.org/10.1016/j.scib.2021.07.013>
- Kay JE et al (2015) The Community Earth System Model (CESM) large ensemble project: a community resource for studying climate change in the presence of internal climate variability. *Bull Am Meteorol Soc* 96(8):1333–1349. <https://doi.org/10.1175/BAMS-D-13-00255.1>
- Lau KM, Kim MK, Kim KM (2006) Asian summer monsoon anomalies induced by aerosol direct forcing: the role of the Tibetan Plateau. *Clim Dyn* 26(7–8):855–864. <https://doi.org/10.1007/s00382-006-0114-z>
- Levy H, Horowitz LW, Schwarzkopf MD, Ming Y, Golaz JC, Naik V, Ramaswamy V (2013) The roles of aerosol direct and indirect effects in past and future climate change. *J Geophys Res Atmos* 118:4521–4532. <https://doi.org/10.1002/jgrd.50192>
- Li Z et al (2016) Aerosol and monsoon climate interactions over Asia. *Rev Geophys* 54:866–929. <https://doi.org/10.1002/2015RG000500>
- Li X, Ting M, Lee DE (2018) Fast adjustment of the Asian summer monsoon to anthropogenic aerosols. *Geophys Res Lett* 45(2):1001–1010. <https://doi.org/10.1002/2017GL076667>
- Li X, Ting M, You Y, Lee DE, Westervelt DM, Ming Y (2020) South Asian summer monsoon response to aerosol-forced sea surface temperatures. *Geophys Res Lett*. <https://doi.org/10.1029/2019GL085329>
- Menary MB et al (2020) Aerosol-forced AMOC changes in CMIP6 historical simulations. *Geophys Res Lett*. <https://doi.org/10.1029/2020GL088166>
- Menon S, Hasen J, Nazarenko L, Luo Y (2002) Climate effects of black carbon aerosols in China and India. *Science* 297:2250–2253. <https://doi.org/10.1126/science.1075159>
- Ming Y, Ramaswamy V, Chen G (2011) A model investigation of aerosol-induced changes in boreal winter extratropical circulation. *J Clim* 24:6077–6091. <https://doi.org/10.1175/2011JCLI4111.1>
- Myhre G et al (2013) Anthropogenic and natural radiative forcing. In: Stocker TF et al (eds) *Climate change 2013: the physical science basis*. Cambridge University Press, Cambridge, pp 659–740
- Oudar T, Kushner PJ, Fyfe JC, Sigmond M (2018) No impact of anthropogenic aerosols on early 21st century global temperature trends in a large initial-condition ensemble. *Geophys Res Lett* 45(17):9245–9252. <https://doi.org/10.1029/2018GL078841>
- Pascoe C, Lawrence BN, Guilyardi E, Juckes M, Taylor KE (2019) Designing and documenting experiments in CMIP6. *Geosci Model Dev Discuss*. <https://doi.org/10.5194/gmd-2019-98>
- Qin M, Dai A, Hua W (2020) Aerosol-forced multidecadal variations across all ocean basins in models and observations since 1920. *Sci Adv* 6(29):eabb0425. <https://doi.org/10.1126/sciadv.abb0425>
- Ranmanathan V et al (2005) Atmospheric brown clouds: impacts on South Asian climate and hydrological cycle. *Proc Natl Acad Sci USA* 102(15):5326–5333. <https://doi.org/10.1073/pnas.0500656102>
- Rosenfeld D et al (2008) Flood or drought: how do aerosols affect precipitation? *Science* 321(5894):1309–1313. <https://doi.org/10.1126/science.1160606>
- Rotstajn LD, Lohmann U (2002) Tropical rainfall trends and the indirect aerosol effect. *J Clim* 15:2103–2116. [https://doi.org/10.1175/1520-0442\(2002\)015%3c2103:TRTATI%3e2.0.CO;2](https://doi.org/10.1175/1520-0442(2002)015%3c2103:TRTATI%3e2.0.CO;2)
- Samset BH, Lund MT, Bollasina M, Myhre G, Wilcox L (2019) Emerging Asian aerosol patterns. *Nat Geosci* 12(8):582–584. <https://doi.org/10.1038/s41561-019-0424-5>
- Santer BD et al (2005) Amplification of surface temperature trends and variability in the tropical atmosphere. *Science* 309(5740):1551–1556. <https://doi.org/10.1126/science.1114867>
- Sen PK (1968) Estimates of the regression coefficient based on Kendall's tau. *J Am Stat Assoc* 63(324):1379–1389. <https://doi.org/10.1080/01621459.1968.10480934>
- Seo J, Kang SM, Frierson DMW (2014) Sensitivity of intertropical convergence zone movement to the latitudinal position of thermal forcing. *J Clim* 27(8):3035–3042. <https://doi.org/10.1175/JCLI-D-13-00691.1>
- Shi JR, Xie SP, Talley LD (2018) Evolving relative importance of the Southern Ocean and North Atlantic in anthropogenic ocean heat uptake. *J Clim* 31(18):7459–7479. <https://doi.org/10.1175/JCLI-D-18-0170.1>
- Soden BJ, Chung ES (2017) The large-scale dynamical response of clouds to aerosol forcing. *J Clim* 30:8783–8794. <https://doi.org/10.1175/JCLI-D-17-0050.1>
- Song F, Zhou T, Qian Y (2014) Response of East Asian summer monsoon to natural and anthropogenic forcings in the 17 latest CMIP5 models. *Geophys Res Lett* 41(2):596–603. <https://doi.org/10.1002/2013GL058705>
- Twomey S (1977) The influence of pollution on the shortwave albedo of clouds. *J Atmos Sci* 34(7):1149–1152. [https://doi.org/10.1175/1520-0469\(1977\)034%3c1149:TIOPOT%3e2.0.CO;2](https://doi.org/10.1175/1520-0469(1977)034%3c1149:TIOPOT%3e2.0.CO;2)
- Undorf S, Bollasina MA, Hegerl GC (2018) Impacts of the 1900–1974 increase in anthropogenic aerosol emissions from North America and Europe on Eurasian summer climate. *J Clim* 31(20):8381–8399. <https://doi.org/10.1175/JCLI-D-17-0850.1>
- Wang L, Liu Q, Xu L, Xie SP (2013) Response of mode water and subtropical countercurrent to greenhouse gas and aerosol forcing in the North Pacific. *J Ocean Univ China* 12(2):191–200. <https://doi.org/10.1007/s11802-013-2193-x>
- Wang Y, Jiang JH, Su H (2015) Atmospheric responses to the redistribution of anthropogenic aerosols. *J Geophys Res Atmos* 120(18):9625–9641. <https://doi.org/10.1002/2015JD023665>
- Wang H, Xie SP, Liu Q (2016a) Comparison of climate response to anthropogenic aerosol versus greenhouse gas forcing: distinct patterns. *J Clim* 29(14):5175–5188. <https://doi.org/10.1175/JCLI-D-16-0106.1>
- Wang H, Xie SP, Tokinaga H, Liu Q, Kosaka Y (2016b) Detecting cross-equatorial wind change as a fingerprint of climate response to anthropogenic aerosol forcing. *Geophys Res Lett* 43(7):3444–3450. <https://doi.org/10.1002/2016GL068521>
- Wang H, Xie SP, Kosaka Y, Liu Q, Du Y (2019) Dynamics of Asian Summer monsoon response to anthropogenic aerosol forcing. *J Clim* 32(3):843–858. <https://doi.org/10.1175/JCLI-D-18-0386.1>
- Wang H, Xie SP, Zheng XT, Kosaka Y, Xu Y, Geng YF (2020) Dynamics of Southern Hemisphere atmospheric circulation response to anthropogenic aerosol forcing. *Geophys Res Lett*. <https://doi.org/10.1029/2020GL089919>
- Wilcox LJ et al (2020) Accelerated increases in global and Asian summer monsoon precipitation from future aerosol reductions. *Atmos Chem Phys* 20(20):11955–11977. <https://doi.org/10.5194/acp-20-11955-2020>
- Xie SP (1996) Westward propagation of latitudinal asymmetry in a coupled ocean–atmosphere model. *J Atmos Sci* 53:3236–3250. [https://doi.org/10.1175/1520-0469\(1996\)053%3c3236:WPO-LAI%3e2.0.CO;2](https://doi.org/10.1175/1520-0469(1996)053%3c3236:WPO-LAI%3e2.0.CO;2)
- Xie SP, Deser C, Vecchi GA, Ma J, Teng H, Wittenberg AT (2010) Global warming pattern formation: sea surface temperature and rainfall. *J Clim* 23(4):966–986. <https://doi.org/10.1175/2009JCLI3329.1>

- Xie SP, Lu B, Xiang B (2013) Similar spatial patterns of climate response to aerosol and greenhouse gas changes. *Nat Geosci* 6(10):828–832. <https://doi.org/10.1038/ngeo1931>
- Xu Y, Xie SP (2015) Ocean mediation of tropospheric response to reflecting and absorbing aerosols. *Atmos Chem Phys* 15(10):5827–5833. <https://doi.org/10.5194/acp-15-5827-2015>
- Zheng B et al (2018) Trends in China's anthropogenic emissions since 2010 as the consequence of clean air actions. *Atmos Chem Phys* 18:14095–14111. <https://doi.org/10.5194/acp-18-14095-2018>

Publisher's Note Springer Nature remains neutral with regard to jurisdictional claims in published maps and institutional affiliations.